The pH-dependent adhesion of nanoparticles to self-assembled monolayers on gold

Journal Item

Available online at www.sciencedirect.com
ScienceDirect
Thin Solid Films xx (2007) xxx–xxx
www.elsevier.com/locate/tsf

The pH-dependent adhesion of nanoparticles to self-assembled monolayers on gold

James Bowen [a], Mayandithevar Manickam [a], Stephen D. Evans [b], Kevin Critchley [b], Kevin Kendall [c,1], Jon A. Preece [a,*]

[a] *School of Chemistry, The University of Birmingham, Edgbaston, Birmingham, B15 2TT, United Kingdom*
[b] *Department of Physics and Astronomy, The University of Leeds, Woodhouse Lane, Leeds, LS2 9JT, United Kingdom*
[c] *Department of Chemical Engineering, The University of Birmingham, Edgbaston, Birmingham, B15 2TT, United Kingdom*

Received 19 March 2007; received in revised form 1 November 2007; accepted 1 November 2007

Abstract

The effect of pH on the adhesion of silica and polystyrene latex nanoparticles, presenting hydroxyl and carboxyl acid surface chemistries respectively, to self-assembled monolayers (SAMs) has been investigated. The SAMs studied were 1-dodecanethiol, 11-mercaptoundecanoic acid and an original pyridine-terminated SAM. Adhesion of nanoparticles to the SAMs was found to decrease with increasing pH due to increased repulsive forces between surfaces, as a result of the deprotonation of surface moieties on the nanoparticles. A range of surface morphologies for the adsorbed nanoparticles was observed for the systems studied.

Keywords: Self-assembled monolayer; Nanoparticle; Adhesion; Surface chemistry; pK_a

1. Introduction

The formation of nanostructures is a prime example of the 'bottom-up' fabrication process and is currently a subject of significant research activity, with number of techniques typically being employed in 'bottom-up' processes. The deposition of nanoparticles onto surfaces is an obvious example of such research, with the ability to assemble nanoparticles into patterns and arrays being one step on the road towards the construction of nanodevices and nanofunctional materials [1]. Mendes et al. [2] discussed the challenge of understanding how ordered or complex structures can form spontaneously by self-assembly, and the problems inherent with controlling such processes. Similarly, Jonas et al. [1] discussed the possible applications of these nanodevices and nanofunctional materials, which include anti-reflective materials [3,4], biosensors [5], and superhydrophobic surfaces [6]. Other examples of 'bottom-up' research include the production of nanopatterned surfaces [7,8], perhaps employing nanolithographic techniques [9]. The formation of deoxyribonucleic acid-mediated artificial nano-biostructures has also been reported [10].

The selective arrangement of nanoparticles on patterned surfaces displaying two or more surface chemistries has been reported by a number of authors. For example, Krüger et al. [11] reported the pH-selective adsorption of latex nanoparticles onto photolithographically patterned silane self-assembled monolayers (SAMs), while Mendes et al. [12] reported the preferential adsorption of citrate-passivated Au nanoparticles onto NH_2-terminated regions of a chemically modified NO_2-terminated silane SAM, which had been patterned using e-beam lithography. Au and Ag nanoparticles have been used in this research area [13] as they can be passivated with thiols and can offer a variety of surface chemistries once passivated. For example, thiol-passivated Au nanoparticles, which were first reported by Brust et al. [14], have been employed in the

* Corresponding author.
E-mail address: k.kendall@bham.ac.uk (K. Kendall).
[1] Tel.: +44 121 414 2739; fax: +44 121 414 5377.

0040-6090/$ - see front matter © 2007 Elsevier B.V. All rights reserved.
doi:10.1016/j.tsf.2007.11.002

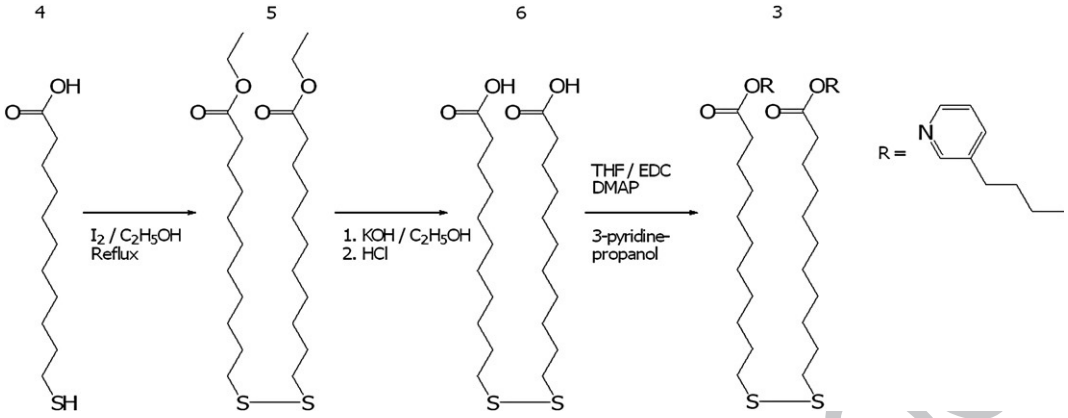

Scheme A1. Synthetic route employed for the synthesis of SAM compound 3. Scheme uploaded electronically.

formation of thin films on silane SAMs, yielding structures with different films providing a range of colours and reflectivities [15].

Nanoparticles are one example of colloidal materials, or colloids. Colloids are found in many aspects of new and old technologies. For example, colloidal clay, polymer latex and calcite particles are used in paper manufacture, each conferring a different function to the finished product. Colloids are found in many other day-to-day items, such as the ink in ball point pens, photocopiers, paints, cosmetics and bricks, and are also an important aspect of biological, medicinal and agricultural systems [16]. The selective deposition of colloids onto surfaces, particularly patterned surfaces, is often controlled by electrostatic, hydrophobic or biospecific interactions [17]. Understanding the mechanisms behind such interactions and the variables which will affect their adhesion is a key part of working towards nanodevices and nanofunctional materials. The work presented here investigates the deposition of colloidal nanoparticles with different surface chemistries onto SAMs which also present a range of surface chemistries. These studies are performed over the pH range 1–11, as pH is often an important parameter in controlling the adhesion between surfaces [7].

2. Experimental details

2.1. Chemical reagents

Three SAM compounds were employed for the deposition of SAMs on Au. 11-mercaptoundecanoic acid (1, Sigma, UK) and 1-dodecanethiol (2, Sigma, UK) were used as received. An original dialkyl disulfide (3) containing a terminal pyridine moiety was synthesised as described in the appendix, the synthetic route being shown in Scheme A1. The structures, contact angle behaviour and the pK_as (in aqueous solution) of the terminal moieties of the SAMs are listed in Table 1. For the pyridine-terminated SAM a prediction of the terminal moiety pK_a was made using the Hammett and Taft equations for heteroaromatic acids and bases [18]. The assumed terminal pK_as for the other SAMs were based on their shorter chain analogues, whose pK_as are well established, because inductive effects fall off rapidly with distance in saturated hydrocarbons [18]. Therefore, the terminal methyl moiety of a 1-dodecanethiol SAM was assumed to have a pK_a of 50 in aqueous solution, analogous to ethane [19]. Likewise, the terminal carboxylic acid moiety of a 11-mercaptoundecanoic acid SAM was assumed to have a pK_a of 4.75 in aqueous solution, analogous to ethanoic acid [20,21].

The organic solvent used for SAM formation was HPLC grade ethanol (Fisher Scientific, UK). Piranha solution was used for glassware cleaning and for cleaning Au slides prior to SAM formation. Piranha solution was made as a 3:7 mixture of 30% laboratory reagent grade hydrogen peroxide (Fisher Scientific, UK) and analytical reagent grade concentrated sulfuric acid (Fisher Scientific, UK). Piranha solution is a very strong oxidising agent and has been known to detonate spontaneously upon contact with organic material. Therefore, eye protection (Fisher Scientific, UK) and nitrile gloves (Bodyguards, UK) were worn at all times, and as a precaution H_2O ice was used as a quenching agent.

Table 1
Chemical structures of SAM compounds 1–3, their H_2O contact angle behaviour and terminal moiety pK_as in aqueous solution

SAM compound	1	2	3
Compound structure	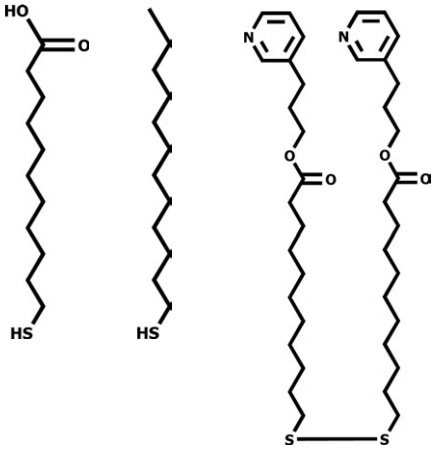		
θ_a (°)	8±3	113±2	54±4
θ_r (°)	~0	95±2	20±4
pK_a of terminal moiety	4.75	50	5.60

Please cite this article as: J. Bowen, et al., Thin Solid Films (2007), doi:10.1016/j.tsf.2007.11.002

When required for pH adjustments, NaOH solutions were made by dissolving NaOH pellets (Fisher Scientific, UK) in Ultra-High Quality (UHQ) H_2O at room temperature, followed by dilution as required. HCl solutions were made by diluting 11.65 M HCl solution (Fisher Scientific, UK) with UHQ H_2O at room temperature. All pH measurements were performed using an IQ150 pH meter (IQ Scientific Instruments) operating at room temperature.

2.2. Deposition of Au thin films and formation of SAMs

Au was deposited onto clean glass microscope slides (BDH, UK) by thermal evaporation using an Auto 306 vacuum evaporation chamber (Edwards, UK). Cr was used as an adhesion promoter, as priming the glass surface with Cr or Ti improves adhesion of Au, which has been reported by various authors when describing their preparation of Au films [8,22–30]. The chamber pressure was reduced to $\sim 10^{-5}$ Pa using a two-stage pumping system. Cr pieces of 99.99% purity (Agar Scientific, UK) were heated by electrical resistance using a voltage of 30 V and a current of 3 A until ~5 nm of Cr had been deposited onto the glass surface. Au wire of 99.99+% purity (Advent Research Materials, UK) of 0.5 mm diameter was placed into a Mo boat (Agar Scientific, UK) and was heated by electrical resistance using a voltage of 10 V and a current of 3 A until ~100 nm of Au had been deposited onto the desired surface. Deposition was monitored using an *in situ* quartz crystal microbalance thickness monitor. The deposition rate for both Cr and Au was in the range 0.05–0.10 nm s^{-1}. Nitrile gloves (Bodyguards, UK) were worn during all handling procedures and Dumostar tweezers (Agar Scientific, UK) were employed to minimise contact with the samples whenever it was practical to do so. Where Au substrates were required to be cut up into smaller pieces, a diamond-tipped scriber (Agar Scientific, UK) was used. Any dust produced was blown away with Ar gas.

All glassware used in SAM formation was cleaned prior to use by immersion in piranha solution at room temperature for ~1 h. Cleaning with piranha solution was followed by rinsing with copious amounts of 18 MΩ deionised H_2O (Elga UHQ-PS) and drying in an oven at 140 °C. SAMs were prepared by immersing Cr-primed, Au-coated glass microscope slides in 1 mM solutions of the SAM compounds for 24 h (11-mercaptoundecanoic acid and 1-dodecanethiol) and 48 h (pyridine SAM compound), using ethanol as a solvent. All Au substrates were cleaned prior to SAM formation by immersion in piranha solution at room temperature for 10 min. Cleaning with piranha solution was followed by rinsing with copious amounts of 18 MΩ deionised H_2O (Elga UHQ-PS) and rinsing with copious amounts of ethanol. After the desired immersion time, Au substrates were removed from the SAM solution and rinsed with copious amounts of ethanol, before being blown dry using Ar gas.

2.3. SAM characterisation procedures

Characterisation of SAMs formed on Au substrates involved assessing their wetting behaviour, elemental composition and thickness, employing dynamic water contact angle measurements, X-ray photoelectron spectroscopy (XPS) and ellipsometry, respectively. Figs. A1–A3 show the XPS spectra obtained for SAMs 1–3 respectively, while Table A1 lists the SAM thicknesses measured using ellipsometry.

Dynamic H_2O contact angles were measured using a home-made stage apparatus, employing a Charge-Coupled Device (CCD) KP-M1E/K camera (Hitachi) and FTA Video Analysis software v1.96 (First Ten Angstroms) for analysis of the contact angle of a droplet of UHQ H_2O at the three-phase intersection point. All data was collected at room temperature and pressure under ambient humidity conditions. A 25 μL gastight syringe (Hamilton) was used for changing the volume of the droplet for all measurements, allowing volume adjustments of ~1 μL to be performed manually, if necessary. The droplet was released onto the sample surface from a blunt-ended needle of ~1 mm diameter (Hamilton). Frames for the video analysis were captured at a rate of 0.12 Hz, usually yielding a minimum of ten frames for both the advancing contact angle and the receding contact angle. Mathematical analysis of the contact angle was performed assuming a non-spherical droplet shape, with manual designation of the baseline for each surface analysed. Data for the advancing contact angle were only chosen when the droplet width was increasing. Similarly, data for the receding contact angle were only chosen when the droplet width was decreasing. The calculated contact angles for each frame during the advancing or receding droplet movement were averaged to give mean values for both the advancing and receding contact angle behaviour of the surface. A minimum of 7 measurements were performed for each sample.

Ellipsometry measurements were performed using a spectroscopic ellipsometer (Jobin-Yvon/Horiba) operating with DeltaPsi2 v2.0.8 software. Ellipsometer calibration and alignment of the Polariser and Detector were performed using an Al reference sample, which has a thermally grown Al_2O_3 layer. The angle of incidence between the analyser and the polariser was set to 70° and was maintained for all subsequent measurements. The light wavelength range used for all measurements was 280–800 nm. All measurements were made under conditions of ambient temperature, pressure and humidity. SAM thicknesses are averages of a minimum of six measurements, each made at a different location on the substrate. Precautions were made to

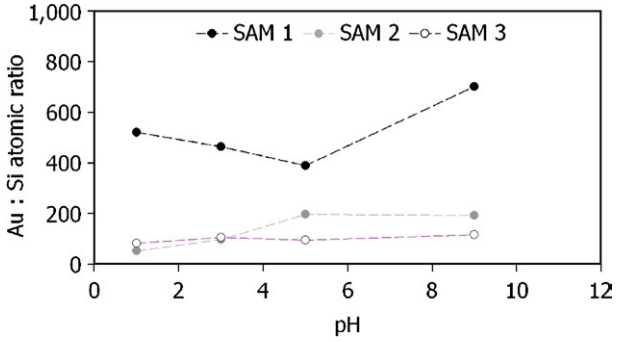

Fig. 1. XPS results for SiO_2 nanoparticles deposited onto SAMs 1–3: Au:Si peak area ratio.

Please cite this article as: J. Bowen, et al., Thin Solid Films (2007), doi:10.1016/j.tsf.2007.11.002

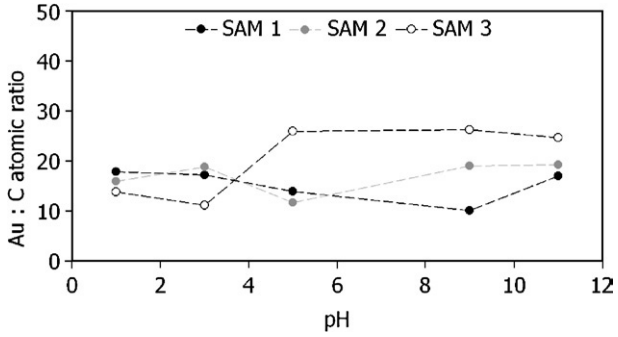

Fig. 2. XPS results for COOH–PL nanoparticles deposited onto SAMs 1–3: Au: C peak area ratio.

avoid performing measurements on visibly defective locations on the sample. Mathematical modelling of the SAM thickness was performed for each measurement. The SAM thickness calculations were based on a three-phase ambient/SAM/Au model, in which the SAM was assumed to be isotropic and assigned an initial refractive index of 1.50 [31–33]. The refractive index of a SAM has also been reported as 1.45 [34,35]. However, it was found that whether the starting value for the iterative calculation process was 1.45 or 1.50, the outcome of the modelling process did not vary. The SAM was modelled using a Cauchy transparent layer, whose initial thickness was varied using a multiguess iterative calculation procedure. The single outcome of each iteration process was the result with the lowest χ^2. A minimum of five different initial values for the SAM thicknesses were chosen for each SAM measurement. Those results with the lowest χ^2 for each measurement made were averaged to give a mean SAM thickness.

XPS analysis of SAMs was performed using an Escalab 250 system (Thermo VG Scientific) operating with Avantage v1.85 software. An Al Kα X-ray source was used, providing a monochromatic X-ray beam with incident energy of 1486.68 eV. All measurements were made at a pressure of $\sim 5 \times 10^{-9}$ mbar. A circular spot size of ~ 0.2 mm^2 was employed throughout all measurements. Samples were immobilised onto stainless steel sample holders, using both double-sided carbon sticky tape (Shintron tape, Shinto Paint Company) and stainless steel or copper sample clips (Thermo VG Scientific). The use of clips provided conductivity between the sample surface and the sample holder, because although the Au film is conductive, the glass substrate is insulating. By providing a conductive link between the sample surface and the sample holder, surface charge retention during measurement was minimised.

Low resolution survey spectra were obtained using a pass energy of 150 eV over a binding energy range of −10 eV to 1200 eV, obtained using 1 eV increments. Recorded low resolution spectra would typically be an average of 5 scans. All

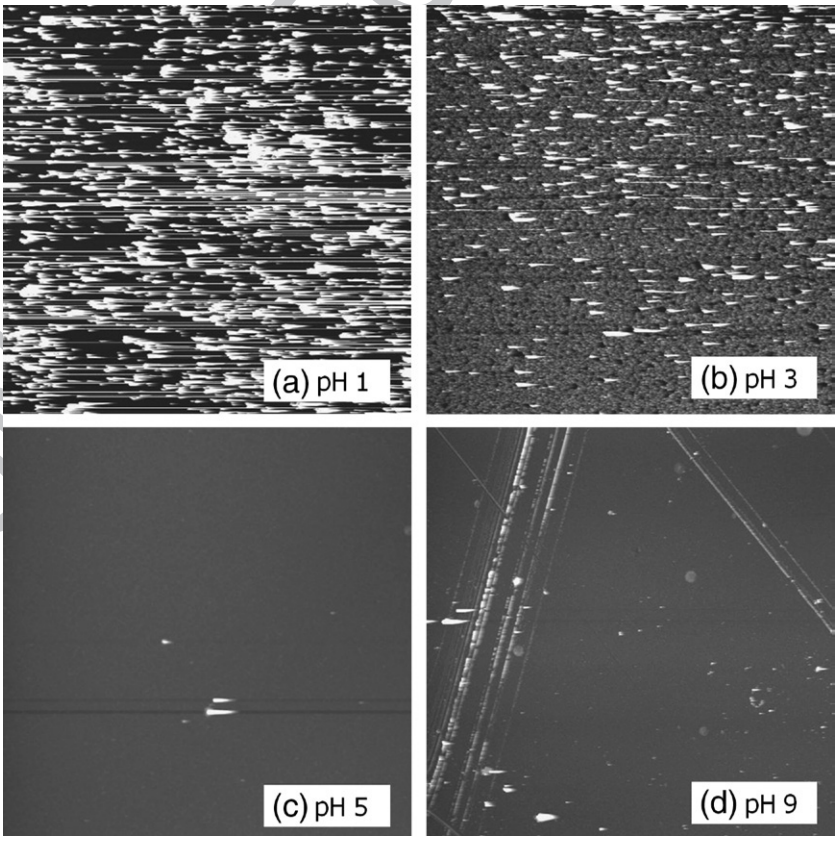

Fig. 3. 50 μm × 50 μm AFM images for SiO_2 nanoparticles deposited onto SAM 1 at pH 1–9 (height scale is 100 nm).

Please cite this article as: J. Bowen, et al., Thin Solid Films (2007), doi:10.1016/j.tsf.2007.11.002

high resolution spectra were obtained using a pass energy of 20 eV over a binding energy range of 20–30 eV, centred around a chosen photoelectron binding energy, obtained using 0.1 eV increments. A dwell time of 20 ms was employed when collecting data from each binding energy increment for all measurements. Recorded high resolution spectra would typically be an average of at least 10 scans.

2.4. Nanoparticle deposition and sample analysis procedures

Two types of nanoparticles were deposited onto SAMs. The nanoparticles were used as received (0.5 g in 10 mL suspension) and were SiO_2 (160 nm diameter, Bangs Labs, USA) and COOH-terminated polystyrene latex (PL) (40 nm diameter, Bangs Labs, USA). Deposition was performed over the pH range 1–11 for the polystyrene latex nanoparticles, but over the pH range 1–9 for the SiO_2 nanoparticles, because SiO_2 dissolves at pH>10 [36]. In each case, 0.1 mL of nanoparticle suspension was added to 20 mL of aqueous solution at the desired pH. Each SAM was immersed in the nanoparticle solution for 2 h before being removed, whereupon it was rinsed with aqueous solution of the same pH as the immersion solution, followed by drying under a stream of Ar gas.

Samples were analysed using atomic force microscopy (AFM) using a Dimension 3100 Nanoscope AFM (Veeco, UK) operating in tapping mode under ambient conditions. The AFM

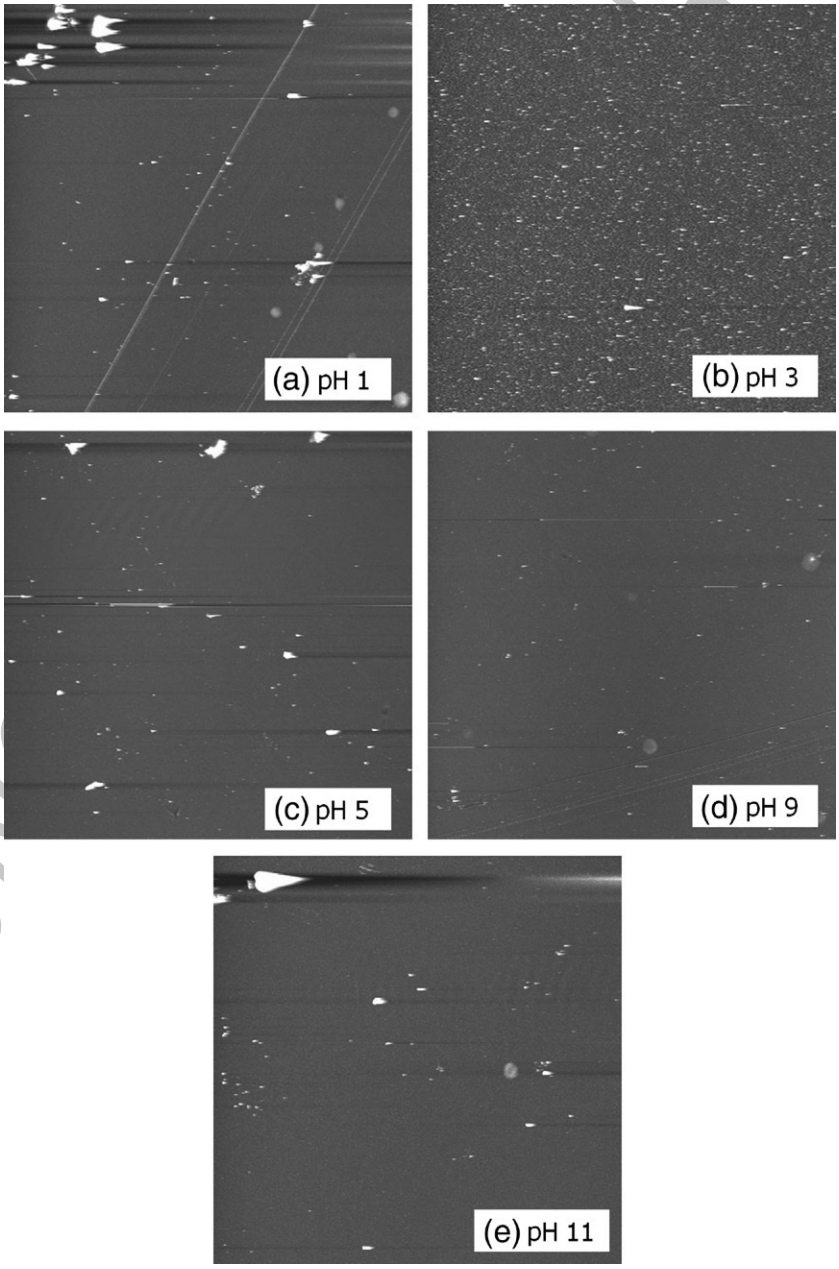

Fig. 4. 50 μm×50 μm AFM images for COOH–PL nanoparticles deposited onto SAM 1 at pH 1–11 (height scale is 100 nm).

was housed on a vibration isolation table to minimise the effect of ambient noise on imaging quality. Nanoscope v5.12 software (Veeco, UK) was used throughout for both real-time analysis and post-capture image processing. Tapping Mode AFM imaging was performed using rectangular 180 μm length pyramidal-tipped Si cantilevers (Veeco, UK) with nominal spring constants of 40 N m^{-1} and resonant frequencies in the range 250–350 kHz. All images were acquired at scan rates between 0.2–2.0 Hz, each image being composed of 512×512 pixels. Samples were immobilised onto steel SPM specimen disks (Agar Scientific, UK) using double-sided sticky tape (3M, UK) prior to AFM analysis. All sample handling was carried out using Dumostar tweezers (Agar Scientific, UK) to minimise the risk of sample contamination.

Samples were analysed by XPS as described in Section 2.3. The area of the Au 4f photoelectron peaks from the Au surface was calculated from the spectra recorded from all samples. For those samples with SiO_2 nanoparticles adhered on them, the area of the Si 2p photoelectron peaks was calculated. Similarly, for those samples with COOH–PL nanoparticles adhered on them, the area of the C 1 s photoelectron peaks was calculated. The contribution to the C 1 s photoelectron peaks from the underlying SAM was assumed to be negligible in comparison to the contribution from the COOH–PL nanoparticles. The Au:Si or Au:C ratios for each SAM/nanoparticle/pH combination were then calculated using relative sensitivity factors according to Wagner et al. [37].

3. Results and discussion

The adhesion of SiO_2 nanoparticles and COOH–PL nanoparticles to SAMs 1–3 is presented in the following sections. The Au:Si ratios for the SAM/SiO_2 nanoparticle systems, and the Au:C ratios for the SAM/COOH–PL nanoparticle systems, as determined by XPS, are presented in Figs. 1 and 2 respectively.

3.1. SAM 1 (carboxylic acid-terminated)

SAM 1 presents a terminal carboxylic acid moiety with an assumed pK_a of 4.75 in aqueous solution. Therefore the pH of the aqueous electrolyte from which the nanoparticles are deposited will determine the protonation state of the SAM and may affect the observed patterns of adhesion. Figs. 3 and 4 show the AFM images SiO_2, COOH–PL and R_3N–PL nanoparticle adhesion to SAM 1 as a function of pH.

Fig. 3 reveals that there is significant adhesion of SiO_2 nanoparticles to SAM 1 at pH 1 and pH 3, while at pH 5 and pH 9 there is little adhesion of SiO_2 nanoparticles. Such behaviour suggests that as the pH increases from 3 to 5 the dissociation of the SiOH groups on the SiO_2 nanoparticles introduces a sufficiently repulsive interaction to prevent adhesion of SiO_2 nanoparticles to the SAM through hydrogen bonding. Similarly, at pH 5 the terminal COOH groups of the SAM may have

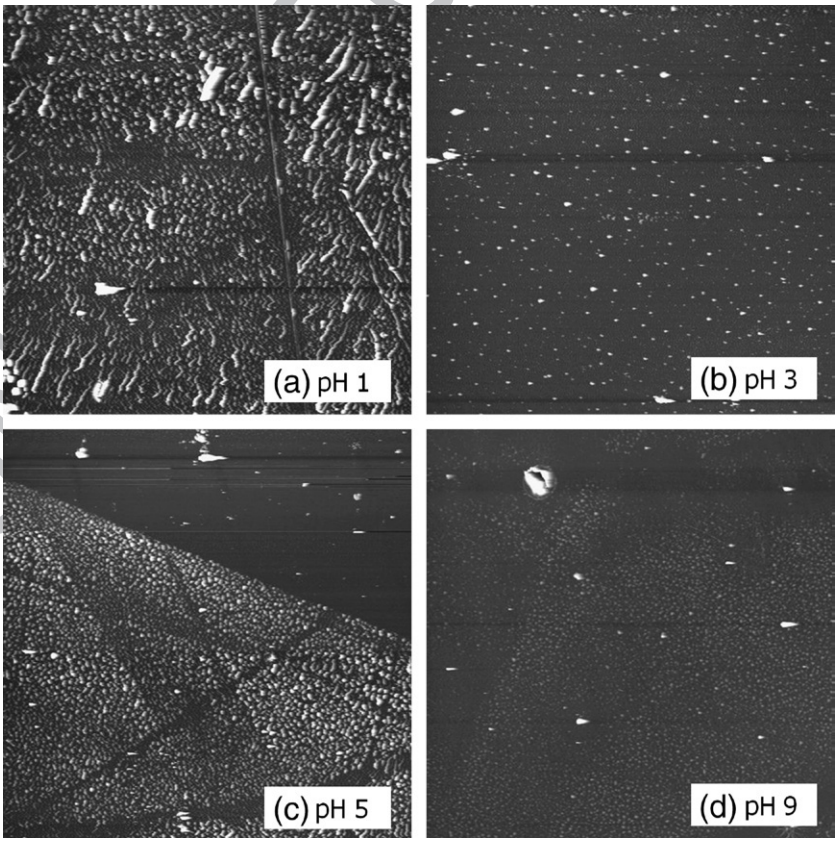

Fig. 5. 50 μm×50 μm AFM images for SiO_2 nanoparticles deposited onto SAM 2 at pH 1–9 (height scale is 100 nm).

Please cite this article as: J. Bowen, et al., Thin Solid Films (2007), doi:10.1016/j.tsf.2007.11.002

dissociated to the carboxylate anion, which would further increase the repulsive interaction between the SiO_2 nanoparticles and the SAM. However, the dissociation of the COOH moiety in SAMs has been investigated by Smith et al. [38,39] and has been reported to increase from 4.75 towards 8.0. The SiO_2 nanoparticle surface consists of hydrophilic SiOH (silanol) groups [40], at a density of 4-5 SiOH groups nm^{-2} [36]. SiO_2 has a negative zeta potential in aqueous solution at pH > 3.5, due to the dissociation of SiOH groups to SiO^-, and the zeta potential will become increasingly negative as pH increases, causing the electrostatic repulsion between nanoparticles to increase. Nevertheless, for the system investigated here it is anticipated that a repulsive interaction will exist between the SAM and the SiO_2 nanoparticles whether the SAM surface consisted of either dissociated or undissociated COOH moieties. The Au:Si ratios obtained from XPS analysis, as shown in Fig. 1, do not agree entirely with the results of the AFM analyses, but it is believed that the morphology of the nanoparticles is a contributory factor in this situation. The aggregation of SiO_2 nanoparticles on the SAM, at pH 1 in particular, may give rise to a higher Au:Si ratio than might be expected, as Si 2p photoelectrons leaving the surface will have to pass through a substantially greater amount of surface material than the Au 4f photoelectrons leaving the surface. Hence, the Au:Si ratio appears to be higher than it actually is. A similar situation may also have occurred at pH 3, at which pH

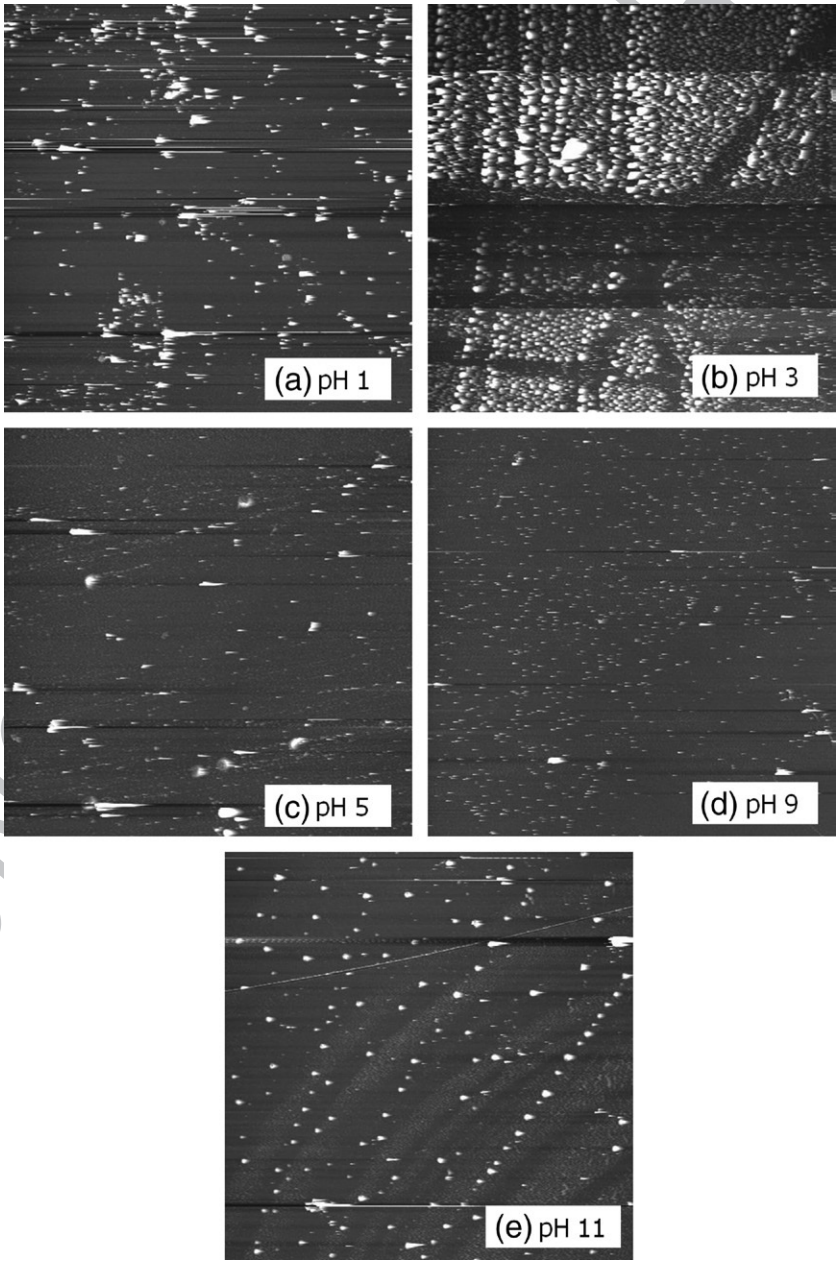

Fig. 6. 50 μm × 50 μm AFM images for COOH–PL nanoparticles deposited onto SAM 2 at pH 1–11 (height scale is 100 nm).

aggregation was also observed, although the nanoparticle aggregates appeared more loosely bound together, which lead to the streaking visible in the AFM image for these pHs.

Figs. 2 and 4 reveal that COOH–PL nanoparticles exhibit little adhesion to SAM 1 at all pHs. However, it would appear from Fig. 2 that there are slightly more COOH–PL nanoparticles adhered to the SAM at pHs 5 and 9 than at the other pHs, which suggests that adhesion was greatest at those pHs around the pK_a of the COOH moiety.

3.2. SAM 2 (methyl-terminated)

SAM 2 presents a terminal methyl moiety with an assumed pK_a of 50 in aqueous solution. Therefore the pH of the aqueous electrolyte from which the nanoparticles are deposited will not affect the protonation state of the SAM, and will not affect the adhesion. Figs. 5 and 6 show the AFM images for SiO_2 and COOH–PL nanoparticle adhesion to SAM 2 as a function of pH.

Figs. 1 and 5 reveal that adhesion of SiO_2 nanoparticles to the methyl-terminated SAM surface occurs at pH 1–9 and decreases somewhat with increasing pH. There is no electrostatic repulsion between the SAM and the SiO_2 nanoparticles, due to the nature of the methyl moiety, hence the adhesion of SiO_2 nanoparticles to the SAM will be dominated by van der Waals forces.

Figs. 2 and 6 reveals that the adhesion of COOH–PL nanoparticles to SAM 2 varies little with pH, although the AFM images indicate differences in the morphology of the deposited COOH–PL nanoparticles, particularly at pH 3. It may be that at pH 3 there exists insufficient electrostatic repulsion between the COOH–PL nanoparticles to prevent aggregation and deposition onto the SAM. At all other pHs, adhesion of COOH–PL nanoparticles to the SAM will be dominated by van der Waals forces.

3.3. SAM 3 (pyridine-terminated)

SAM 3 presents a terminal pyridine moiety with a predicted pK_a of 5.60 in aqueous solution. Therefore the pH of the aqueous electrolyte from which the nanoparticles are deposited will determine the protonation state of the SAM. Figs. 7 and 8 show the AFM images for SiO_2 and COOH–PL nanoparticle adhesion to SAM 3 as a function of pH.

Fig. 1 reveals that as pH increases the Au:Si ratio remains approximately constant, which suggests that the adhesion of SiO_2 nanoparticles to SAM 3 remained approximately constant with pH. This is in contrast to the AFM results, presented in Fig. 7, which reveal that as pH increases the number of SiO_2 nanoparticles deposited decreases. It is believed that the morphology of the nanoparticles is a contributory factor in this situation, as discussed for SAM 1. Briefly, the aggregation of SiO_2 nanoparticles on the SAM increases the amount of surface material which the photoelectrons leaving the surface must pass through before being detected, which can serve to

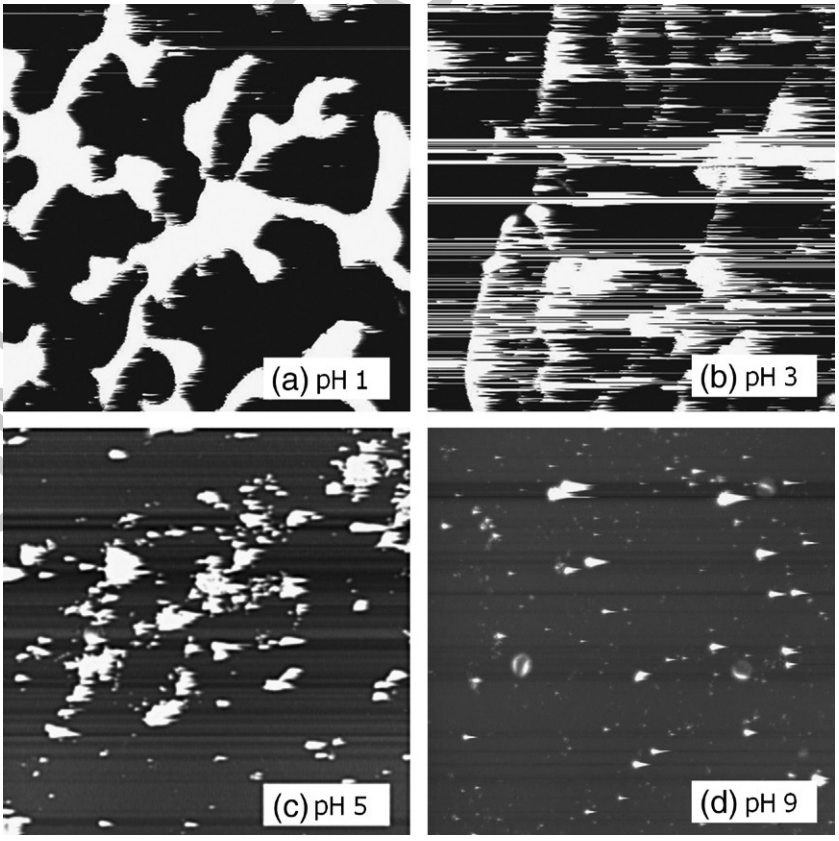

Fig. 7. 50 μm × 50 μm AFM images for SiO_2 nanoparticles deposited onto SAM 3 at pH 1–9 (height scale is 100 nm).

Please cite this article as: J. Bowen, et al., Thin Solid Films (2007), doi:10.1016/j.tsf.2007.11.002

distort the measured photoelectron counts. At pH 1 and pH 3 it would be expected that the SiO_2 nanoparticles have a little or no surface charge, and therefore the observed aggregation of the SiO_2 nanoparticles, leading to the deposition of aggregates on the SAM, might also be expected. At pH 5 and pH 9 the SiO_2 nanoparticles will exhibit negatively charged surfaces and therefore will repel each other, preventing aggregation. The terminal pyridinium moieties of SAM 3 will become increasingly dissociated with increasing pH, which will serve to decrease the cationic surface charge of the SAM. This decreasing surface charge will also promote the adhesion of fewer SiO_2 nanoparticles to the SAM.

Fewer SiO_2 nanoparticles are adsorbed onto SAM 1 than to SAMs 2 and 3, particularly at pH > 5, due to the deprotonation of both the SiO_2 nanoparticle surface and the SAM terminal moieties, leading to electrostatic repulsion between the SAM and the SiO_2 nanoparticles, preventing adhesion. For SAM 2 there will be no deprotonation of its terminal moieties with increasing pH. For SAM 3, the deprotonation of the terminal pyridine moiety will still leave a surface capable of some electrostatic attraction with the SiO_2 nanoparticles. Therefore, only SAM 1 does not present a surface capable of adhering SiO_2 nanoparticles at increased pH.

Fig. 2 reveals that the Au:C ratio increases with increasing pH, suggesting a decrease in adhesion of COOH–PL nanoparticles to SAM 3 between these pHs. This trend is in approximate agreement with the AFM results, presented in

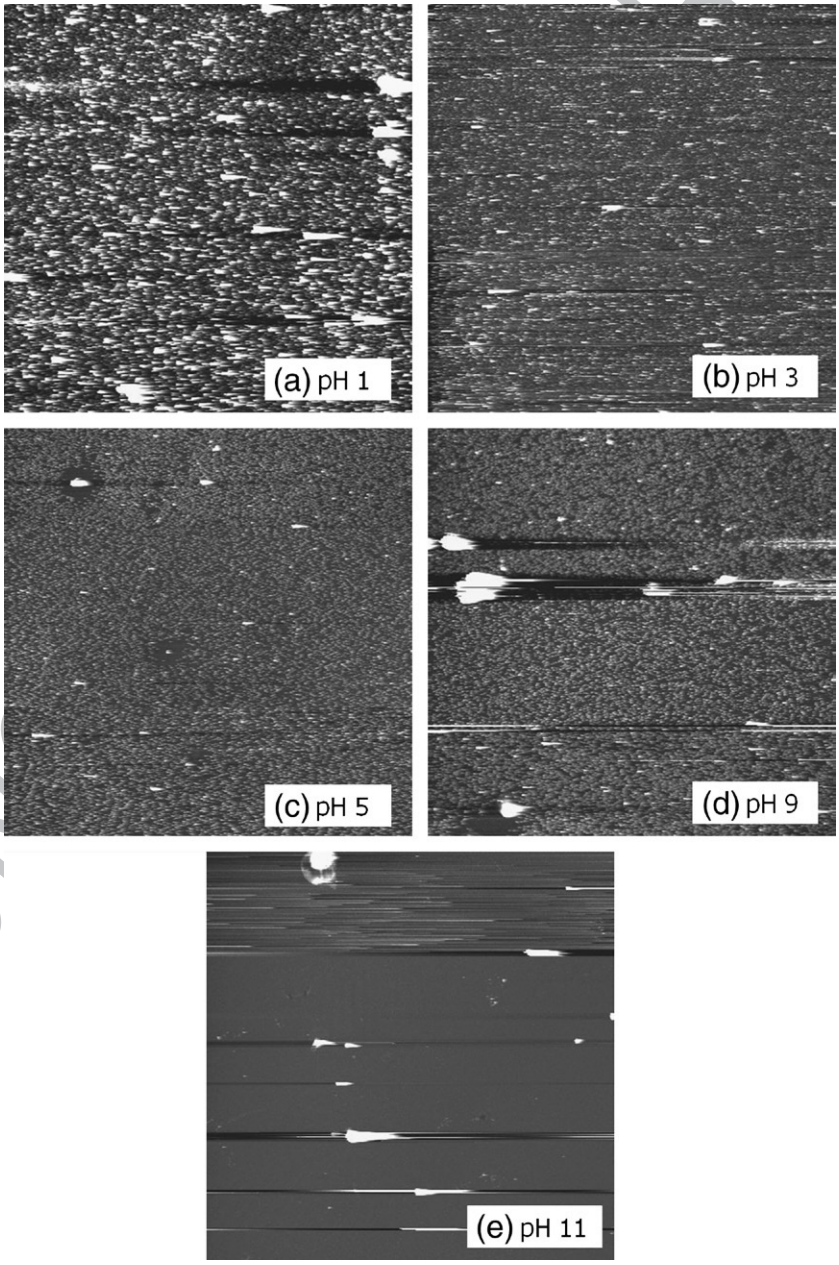

Fig. 8. 50 μm × 50 μm AFM images for COOH–PL nanoparticles deposited onto SAM 3 at pH 1–11 (height scale is 100 nm).

Fig. 8. The decreasing adhesion of COOH–PL nanoparticles to SAM 3 with increasing pH may be linked to the increasing dissociation of the surface COOH groups on the COOH–PL nanoparticles with increasing pH. Adhesion of COOH–PL nanoparticles to the SAM is reduced at pHs above the pK_a of the COOH moiety, although the apparent pK_a of the moiety, which is 4.75 in free solution, has been shown to increase when present at a surface [38,39], for example when it is the surface moiety of a SAM. For both the XPS and the AFM data, the decrease in adhesion of COOH–PL nanoparticles to the SAM occurs at pH greater than the pK_a of the COOH moiety.

4. Conclusions

The effect of electrolyte pH on the deposition and adhesion of nanoparticles to SAMs presenting carboxylic acid, methyl and pyridine surface moieties has been investigated using AFM and XPS. Adhesion was found to vary with pH for many combinations of SAM and nanoparticle, with a number of different surface morphologies of nanoparticles being observed. The adhesion behaviour is believed to be linked to the protonation state of the surface moieties on the nanoparticles, rather than simply the contact angle behaviour of the SAM, whereby increasing pH often led to decreased nanoparticle adhesion, probably due to increased repulsive interactions between the SAMs and the nanoparticle, and also between nanoparticles. Differences in nanoparticle adhesion were observed between SAMs for the same nanoparticle and pH, due to the different surface properties of each SAM, such as pK_a. Further investigation on systems such as these could include the study of nanoparticle adhesion to hydroxyl-terminated SAMs and assessment of the mass of adhered nanoparticles using a quartz crystal microbalance.

Acknowledgements

We acknowledge The University of Birmingham and ACORN (A Collaboration on Research into Nanoparticles) for financial support. We also acknowledge the assistance and advice given by Professor G.J. Leggett and Dr. S. Sun at the University of Sheffield, School of Chemistry.

Appendix A

The following supporting information is presented. (i) Synthesis and characterisation data for SAM compound 1. (ii) Characterisation results for SAMs 1–3, consisting of elemental composition as determined by X-ray photoelectron spectroscopy and thickness data as determined by ellipsometry.

A.1. Synthesis and characterisation data for SAM compound 3

A.1.1. Compound 5

To a solution of 11-mercaptoundecanoic acid 4 (7.0 g, 32.1 mM) in C_2H_5OH (100 mL) heated under reflux was added a solution of iodine (4.07 g, 16.03 mM) in C_2H_5OH (50 mL). Heating was continued for 12 h after which the reaction was allowed to cool to room temperature and washed with a saturated aqueous solution of $Na_2S_2O_3$ (50 mL). The products were extracted into CH_2Cl_2 (3×50 mL) and dried ($MgSO_4$), filtered and the solvent was removed *in vacuo*. The residues were purified by recrystallisation from CH_2Cl_2/hexane. The feathery white crystals were filtered from the mother liquor, washed with ice-cold hexane and dried *in vacuo* affording 5 (6.47 g, 82%). *m/z* (ES) 513 $[M+Na]^+$ δ_H (500 MHz, $(CD_3)_2SO$) 4.09 (4H, *q*, *J*=7.3, 14.3 Hz), 2.65 (4H, *t*, *J*=7.3 Hz), 2.26 (4H, *t*, *J*=7.3 Hz), 1.61 (8H, m), 1.34 (30H, m). δ_C (400 MHz, $CDCl_3$) 173.9, 60.1, 39.1, 34.4, 29.3, 29.2, 28.5, 24.9, 14.2. Elemental analysis of $C_{26}H_{50}O_4S_2$ requires C 63.67%, H 10.20%. Elemental analysis found C 63.52%, H 10.48%.

A.1.2. Compound 6

To a vigorously stirred solution of 5 (4.75 g, 9.68 mM) in tetrahydrofuran (THF) (100 mL) was added a solution of potassium hydroxide (1.63 g, 29.0 mM) in H_2O/C_2H_5OH (1:1, 20 mL). The reaction was stirred for 12 h, and acidified with HCl (aq, 2 M, 20 mL) upon which a white solid precipitated. The solid was filtered off, washed with H_2O (100 mL), cold C_2H_5OH (100 mL) and dried *in vacuo* affording 6 as white plate-like crystals (4.20 g, 99%). *m/z* (ES) 457 $[M+Na]^+$. δ_H (400 MHz $(CD_3)_2SO$) 3.5 (2H, s), 2.68 (4H, *t*, *J*=8.0 Hz), 2.14 (4H, *t*, *J*=8.0 Hz), 1.62 (4H, m), 1.46 (4H, m), 1.2 (24H,m). δ_C (400 MHz, $(CD_3)_2SO$) 174.5, 38.0, 33.7, 28.9, 28.8, 28.6, 28.6, 27.8, 24.5. Elemental analysis of $C_{22}H_{42}O_4S_2$ requires C 60.82%, H 9.67%. Elemental analysis found C 60.78%, H 9.70%.

A.1.3. Compound 3

To a solution of 6 (0.100 g, 0.23 mM) in dry THF (10 mL) cooled to 0 °C under an N_2 atmosphere was added 1–(3–dimethylaminopropyl)–3–ethyl–carbodiimide hydrochloride (0.272 g, 1.38 mM) and a catalytic amount of 4–dimethyl–aminopyridine. The mixture was stirred for 30 min and 3–pyridinepropanol (0.094 g, 0.69 mM) was added over 10 min, followed by further stirring for 24 h under an N_2 atmosphere at room temperature. The white precipitate was filtered and the filtrate was diluted with CH_2Cl_2 (30 mL) and washed with H_2O (3×30 mL), followed by 10% aqueous $NaHCO_3$ (10 mL) and saturated (aqueous) NaCl (5 mL). The organic phase was dried ($MgSO_4$), filtered and the filtrate evaporated to dryness under reduced pressure. The residue was purified by silica gel column chromatography (eluent: CH_2Cl_2/EtOAc, 3:1) to yield 3 (0.045 g, 29%) as a white solid. *m/z* (ES) 695 $[M+Na]^+$.δ_H (400 MHz, $CDCl_3$) 8.4 (4H, m), 7.47 (2H, m), 7.19 (2H, m), 4.07 (4H, *t*, *J*=6.4 Hz), 2.66 (8H, m), 2.27 (4H, *t*, *J*=8.0 Hz), 1.94 (4H, m), 1.66 (8H, m), 1.32 (24H, m). δ_C (400 MHz, $CDCl_3$) 173.7, 149.9, 147.5, 136.3, 135.6, 123.2, 63.1, 39.0, 34.2, 29.8, 29.3, 29.1, 28.4, 24.9. Elemental analysis of $C_{38}H_{60}O_4N_2S_2$ requires C 67.75%, H 8.91%, N 4.16%. Elemental analysis found C 67.80%, H 8.82%, N 4.07%.

Please cite this article as: J. Bowen, et al., Thin Solid Films (2007), doi:10.1016/j.tsf.2007.11.002

A.2. Characterisation results for SAMs 1–3

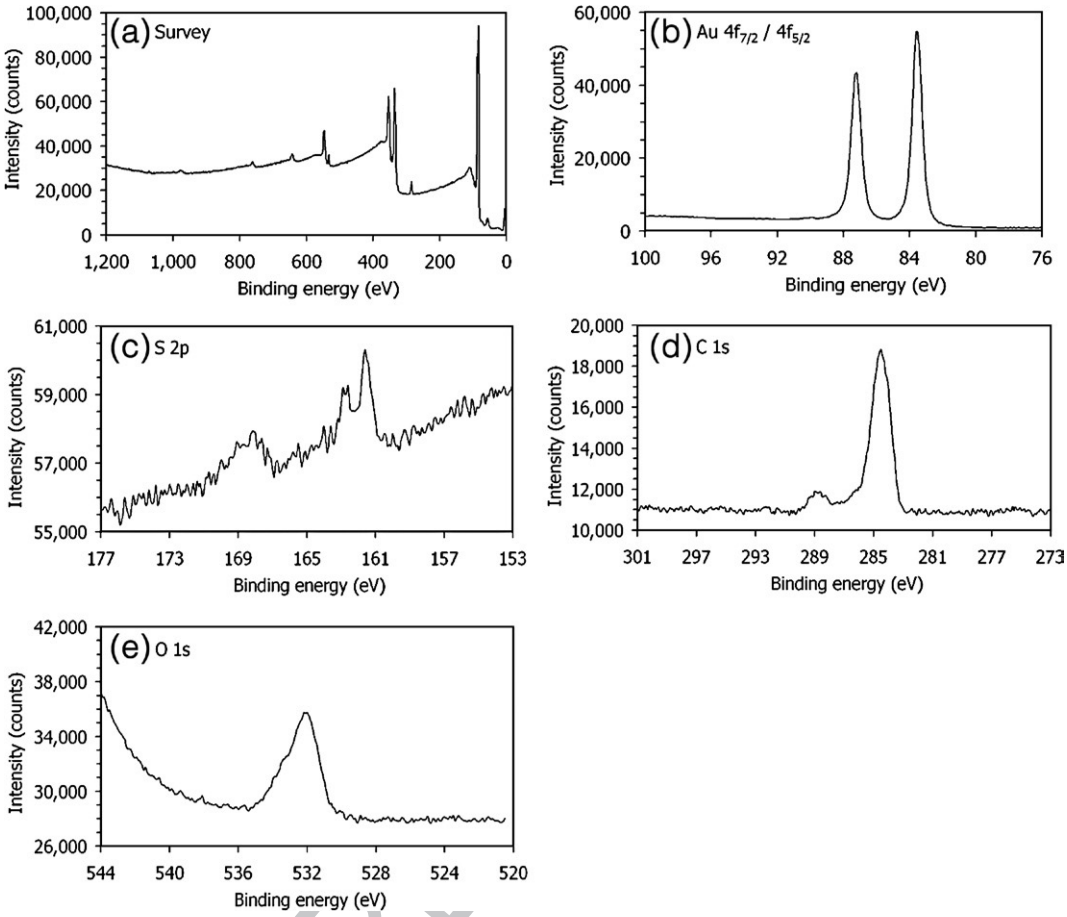

Fig. A1. XPS spectra for SAM 1. Figure uploaded electronically.

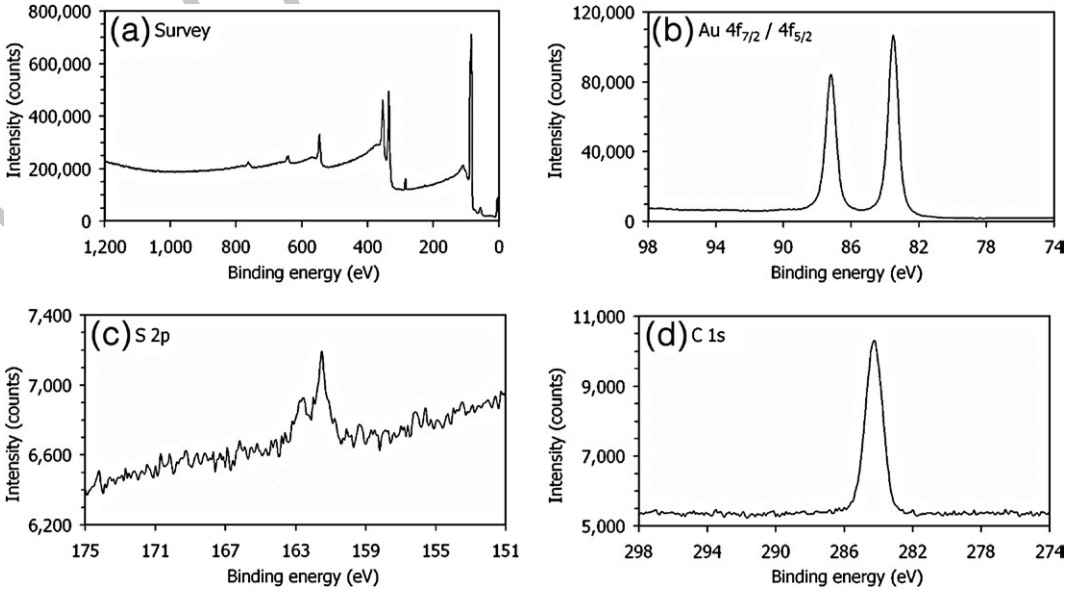

Fig. A2. XPS spectra for SAM 2. Figure uploaded electronically.

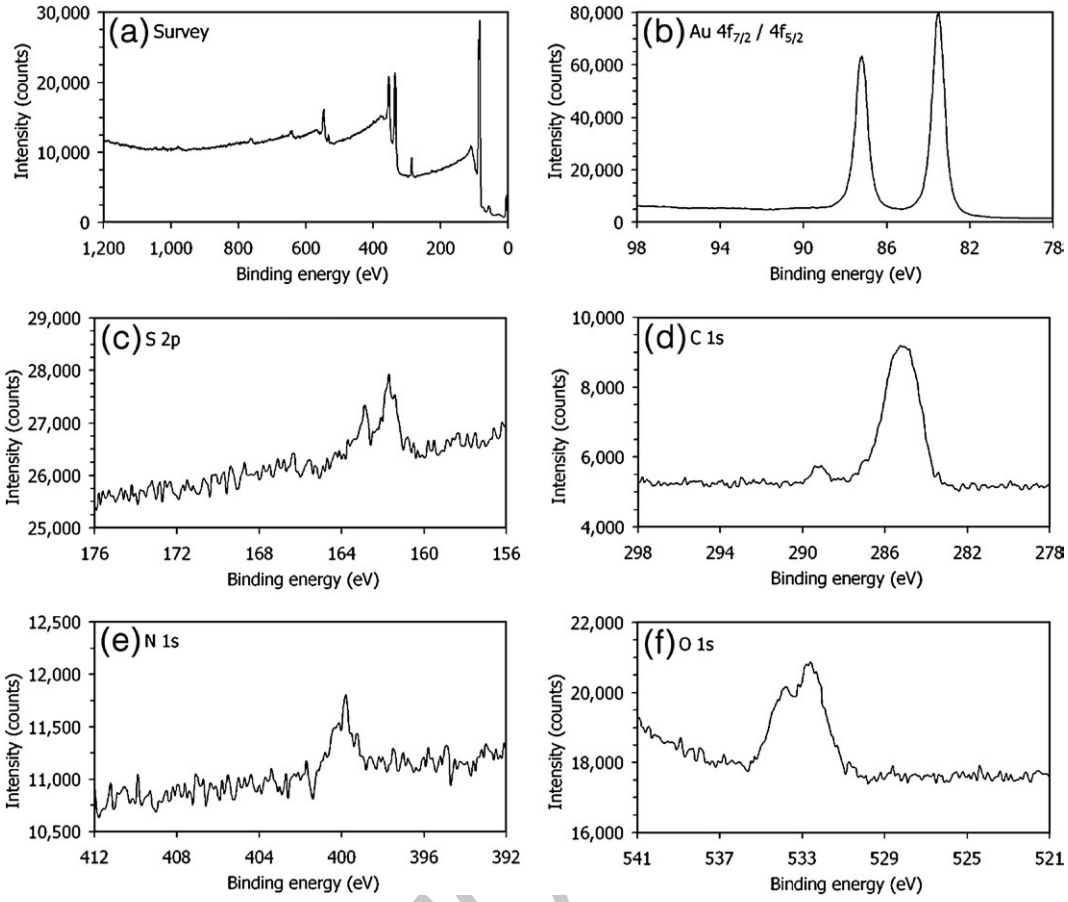

Fig. A3. XPS spectra for SAM 3. Figure uploaded electronically.

Table A1
Ellipsometrically measured thicknesses for SAMs 1–3

SAM	Calculated thickness range (nm)	Measured thickness (nm)
1	1.32–1.53	1.09±0.16
2	1.34–1.55	1.45±0.15
3	1.94–2.24	1.42±0.31

A thickness range for each SAM was calculated by estimating the length of the molecular structures of compounds 1–3 using ChemDraw Ultra (v7.0.1, CambridgeSoft, UK) and Chem3D Ultra (v7.0.0, CambridgeSoft, UK) software. The upper limit of the range is the full length of the SAM molecule. The chosen lower limit of the range is the height of the SAM molecule at a tilt angle of 30° to the surface normal.

References

[1] U. Jonas, C. Krüger, J. Supramol. Chem. 2 (2002) 255.
[2] P.M. Mendes, Y. Chen, R.E. Palmer, K. Nikitin, D. Fitzmaurice, J.A. Preece, J. Phys., Condens. Matter 15 (2003) S3047.
[3] K. Hadobás, S. Kirsch, A. Carl, M. Acet, E.F. Wassermann, Nanotechnology 11 (2000) 161.
[4] H. Hattori, Adv. Mater. 13 (2001) 51.
[5] H.-F. Ji, T. Thundat, Biosens. Bioelectron. 17 (2002) 337.
[6] A. Marmur, Langmuir 20 (2004) 3517.
[7] H.-X. He, W. Huang, H. Zhang, Q.G. Li, S.F.Y. Li, Z.F. Liu, Langmuir 16 (2000) 517.
[8] J.L. Wilbur, H.A. Biebuyck, J.C. MacDonald, G.M. Whitesides, Langmuir 11 (1995) 825.
[9] P.M. Mendes, J.A. Preece, Curr. Opin. Colloid Interface Sci. 9 (2004) 236.
[10] R. Bashir, Superlattices Microstruct. 29 (2001) 1.
[11] C. Krüger, U. Jonas, J. Colloid Interface Sci. 254 (2002) 331.
[12] P.M. Mendes, S. Jacke, K. Critchley, J. Plaza, Y. Chen, K. Nikitin, R.E. Palmer, J.A. Preece, S.D. Evans, D. Fitzmaurice, Langmuir 20 (2004) 3766.
[13] M. Brust, C.J. Kiely, Colloids Surf., A 202 (2002) 175.
[14] M. Brust, M. Walker, D. Bethell, D.J. Schiffrin, R. Whyman, Chem. Commun. (Cambridge U.K.) (1994) 801.
[15] T. Ung, L.M. Liz-Marzán, P. Mulvaney, Colloids Surf., A 202 (2002) 119.
[16] R.J. Hunter, Foundations of Colloid Science, 2nd edition, Oxford University Press, Oxford, 2001.
[17] P.T. Hammond, in: F. Caruso (Ed.), Colloids and Colloid Assemblies: Synthesis, Modification, Organization and Utilization of Colloid Particles, Wiley-VCH, Darmstadt, 2004.
[18] D.D. Perrin, B. Dempsey, E.P. Serjeant, pKa Prediction for Organic Acids and Bases, Chapman and Hall, London, 1981.
[19] pK_a of ethane is given as 50 in T.W.G. Solomons, Organic Chemistry 5th Edition, John Wiley & Sons, New York, 1992.
[20] pK_a of ethanoic acid is given as 4.75 in P.W. Atkins, Physical Chemistry 6th edition, Oxford University Press, Oxford, 1998.
[21] pK_a of ethanoic acid is given as 4.76 in R. Stewart, The Proton: Applications to Organic Chemistry, Academic Press, Orlando, 1985.
[22] D.Y. Petrovykh, H. Kimura-Suda, L.J. Whitman, M.J. Tarlov, J. Am. Chem. Soc. 125 (2003) 5219.
[23] M.-Y. Tsai, J.-C. Lin, J. Colloid Interface Sci. 238 (2001) 259.
[24] V.H. Pérez-Luna, S. Yang, E.R. Rabinovich, T. Buranda, L.A. Sklar, P.D. Hampton, G.P. López, Biosens. Bioelectron. 17 (2002) 71.
[25] C.A. Scotchford, C.P. Gilmore, E. Cooper, G.J. Leggett, S. Downes, J. Biomed. Mater. Res. 59 (2002) 84.

Please cite this article as: J. Bowen, et al., Thin Solid Films (2007), doi:10.1016/j.tsf.2007.11.002

[26] N.J. Brewer, B.D. Beake, G.J. Leggett, Langmuir 17 (2001) 1970.
[27] W.M. Albers, J. Likonen, J. Peltonen, O. Teleman, H. Lemmetyinen, Thin Solid Films 330 (1998) 114.
[28] R.R. Shah, D.M. Heinrichs, N.L. Abbott, Colloids Surf., A 174 (2000) 197.
[29] M.K. Ferguson, E.R. Low, J.R. Morris, Langmuir 20 (2004) 3319.
[30] E.W. van der Vegte, G. Hadziioannou, Langmuir 13 (1997) 4357.
[31] M.D. Porter, T.B. Bright, D.L. Allara, C.E.D. Chidsey, J. Am. Chem. Soc. 109 (1987) 3559.
[32] C.D. Bain, E.B. Troughton, Y.-T. Tao, J. Evall, G.M. Whitesides, R.G. Nuzzo, J. Am. Chem. Soc. 111 (1989) 321.
[33] S.D. Evans, R. Sharma, A. Ulman, Langmuir 7 (1991) 156.
[34] H.A. Biebuyck, C.D. Bain, G.M. Whitesides, Langmuir 10 (1994) 1825.
[35] R. Colorado Jr., R.J. Villazana, T.R. Lee, Langmuir 14 (1998) 6337.
[36] R.K. Iler, The Chemistry of Silica: Solubility, Polymerisation, Colloid and Surface Properties, and Biochemistry, John Wiley and Sons, New York, 1979.
[37] C.D. Wagner, in: D. Briggs, M.P. Seah (Eds.), 2nd Edition, Practical Surface Analysis, vol. 1, J. Wiley & Sons, Chichester, 1990, Appendix.
[38] D.A. Smith, M.L. Wallwork, J. Zhang, J. Kirkham, C. Robinson, A. Marsh, M. Wong, J. Phys. Chem., B 104 (2000) 8862.
[39] M.L. Wallwork, D.A. Smith, J. Zhang, J. Kirkham, C. Robinson, Langmuir, 17 (2001) 1126.
[40] R. Raiteri, B. Margesin, M. Grattarola, Sens. Actuators B 46 (1998) 126.

Please cite this article as: J. Bowen, et al., Thin Solid Films (2007), doi:10.1016/j.tsf.2007.11.002